Hydrol. Earth Syst. Sci. Discuss., 11, 9519–9549, 2014
www.hydrol-earth-syst-sci-discuss.net/11/9519/2014/
doi:10.5194/hessd-11-9519-2014

Hydrology and Earth System Sciences
Open Access
Discussions

Estimates of global dew collection potential

H. Vuollekoski[1], M. Vogt[1,2], V. A. Sinclair[1], J. Duplissy[1], H. Järvinen[1], E.-M. Kyrö[1], R. Makkonen[1], T. Petäjä[1], N. L. Prisle[1], P. Räisänen[3], M. Sipilä[1], J. Ylhäisi[1], and M. Kulmala[1]

[1]University of Helsinki, Department of Physics, Helsinki, Finland
[2]Norwegian Institute for Air Research, Oslo, Norway
[3]Finnish Meteorological Institute, Helsinki, Finland

Received: 24 June 2014 – Accepted: 26 July 2014 – Published: 12 August 2014

Correspondence to: H. Vuollekoski (henri.vuollekoski@helsinki.fi)

Published by Copernicus Publications on behalf of the European Geosciences Union.

Abstract

The global potential for collecting usable water from dew on an artificial collector sheet was investigated by utilising 34 years of meteorological reanalysis data as input to a dew formation model. Dew formation was found to be frequent and common, but daily yields were mostly below 0.1 mm. Nevertheless, some water-stressed areas such as the coastal regions of northern Africa and the Arabian Peninsula show potential for large-scale dew harvesting, as the yearly yield can reach up to 100 $\mathrm{L\,m^{-2}}$ for a commonly used polyethylene foil. Statistically significant trends were found in the data, indicating overall changes in dew yields between ±15 % over the investigated time period.

1 Introduction

The increasing concern over the diminishing and uneven distribution of fresh water resources affects the daily life and even survival of billions of people. The United Nations Development Programme (2006) estimated that there were already 1.1 billion people in developing countries lacking adequate access to water, a figure that is expected to climb to 3 billion by 2025 due to the increasing population particularly in the most water-stressed parts of the planet.

On the other hand, water exists everywhere in one form or another: ground water, rivers, lakes, seas, glaciers, snow, ice caps, clouds, soil, and as air moisture. In particular, air moisture is present everywhere; even the driest of deserts have some, and warm air can contain more humidity than cold air. The absolute quantities of water by volume of air are of course very small (of the order of grams or some tens of grams per cubic meter), and harvesting it may be expensive or technologically demanding – factors that are rarely met in the areas of most immediate need for sustainable sources of water. Nevertheless, if no other sources of usable water exist nearby, harvesting water

HESSD
11, 9519–9549, 2014

from the air might provide an economically sound supply of water for both drinking and agriculture.

Harvesting moisture from the air has two potential pathways: fog and dew. Fog is a highly local phenomenon that occurs, for example, when moist air is cooled by the emission of long-wave radiation or by forced ascent up a mountain slope: the decrease in temperature causes supersaturation and the formation of fog. The droplets may then be harvested by artificial structures resembling tennis nets equipped with rain gutters as has been investigated in many previous studies (e.g. Schemenauer and Cereceda, 1991; Klemm et al., 2012; Fessehaye et al., 2014).

The formation of dew occurs when the temperature of a surface is below the dew point temperature, and water vapour condenses onto the surface. In this study, the surface is assumed to be a macroscopic, artificial structure. Since only a thin layer of air over the surface reaches supersaturation, by volume the formation of dew is a very slow process compared to the formation of fog. Nevertheless, the formation and collection of dew has been studied and has been found to be feasible in several locations around the world (e.g. Vogt et al., 2014). Additionally, material design can affect the characteristics of the condensing surface and improve its efficiency for dew collection. For example, the higher the emissivity of the surface, the higher its rate of cooling by radiation. During nights with clear skies, when both sunlight and thermal radiation from clouds are absent, the incoming radiation may be exceeded by the device's own out-going thermal radiation, resulting in a net cooling.

In this global modelling study we focus on the formation of dew onto an artificial surface, and investigate the potential for its collection. This seemingly arbitrary limitation is based on the following facts: (a) the potential for dew formation is almost ubiquitous regardless of orographic features or presence of water in other forms, (b) the formation of dew can be artificially enhanced with relatively minor efforts, (c) the formation of dew is a well-defined mathematical problem suitable for computer modelling at global scales, and (d) we are unaware of any such previous studies.

HESSD
11, 9519–9549, 2014

The present article describes the implementation of a model for dew formation onto an artificial surface, which is upscaled with meteorological input from a long term reanalysis dataset that spans the years 1979–2012. Modelling 34 years of dew formation ensure that the results are statistically robust. Our model is based on the approach used by e.g. Beysens et al. (2005), who demonstrated that their model could simulate dew yields which agreed well with their measurements taken at three southern European sites.

The dew formation model, forced with reanalysis data, provides spatially coarse (80 km) estimates of dew collection yields for given sheet technologies along with the temporal evolution of dew formation. Therefore, the model output allows global maps of dew formation to be produced and areas which have the potential for large-scale dew collection to be identified. The modelled dew collection estimates can be used as first-order estimates by those who are planning local feasibility studies that include additional factors such as lakes, rivers, and road access. The long time-series of our study provides information about the seasonal variation of dew formation as well as long-term trends in dew yield, which may be associated with climate change.

2 Methods

In order to form global estimates of dew collection potential, we combined a computationally efficient dew formation model with historical, global meteorological reanalysis data spanning 34 years. The offline model was run on a computer cluster with 64 cores, which allowed global model runs with different parametrizations to run in approximately 10 h each.

The program source code, written in Python and Cython, is available at (*to be disclosed after acceptance for publication*).

HESSD
11, 9519–9549, 2014

2.1 Model description

In implementing the model that describes the formation of dew (represented by mass yield of either liquid water or ice), we followed the approach presented by Pedro and Gillespie (1982) and Nikolayev et al. (1996), which has been found to agree well with empirical measurements of dew collection (e.g. Beysens et al., 2005). The algorithm integrates the prognostic equations for the mass and heat balance by turns, thereby describing the temperature of the condenser and the resulting condensation rate onto it. As the model is global and thus incorporates both polar regions, we include the dynamics of water changing phase between liquid and solid. However, for simplicity, here we refer to both phase changes of vapour-to-liquid (condensation) and vapour-to-ice (desublimation) as condensation, and to both liquid and solid phases as water, unless specified otherwise. In our model we consider dew only and the occurrence of precipitation or fog are unaccounted for apart from their potential indirect effects included within the input reanalysis data.

The condenser in our model is a horizontally-aligned sheet of some suitable material, such as low-density polyethylene (LDPE) or polymethylmethacrylate (PMMA), and is thermally insulated from the ground at a height of 2 m. Unless specified otherwise, the particular parameter values used in the model (listed in Table 1) match those of the inexpensive LDPE foil used by e.g. the International Organization for Dew Utilization, whose foil composition follows Nilsson et al. (1994).

The heat equation can be written as:

$$\frac{\mathrm{d}T_\mathrm{c}}{\mathrm{d}t}(C_\mathrm{c}m_\mathrm{c} + C_\mathrm{w}m_\mathrm{w} + C_\mathrm{i}m_\mathrm{i}) = P_\mathrm{rad} + P_\mathrm{conv} + P_\mathrm{lat}, \quad (1)$$

where $T_\mathrm{c}, C_\mathrm{c}$, and m_c are the condenser's temperature, specific heat capacity and mass, respectively. The condenser's mass is given by $m_\mathrm{c} = \rho_\mathrm{c} S_\mathrm{c} \delta_\mathrm{c}$, where $\rho_\mathrm{c}, S_\mathrm{c}$ and δ_c are its density, surface area (here 1 m^2) and thickness (see Table 1). C_w and m_w are the specific heat capacity and mass of liquid water, representing the cumulative mass

HESSD
11, 9519–9549, 2014

of water that has condensed onto the sheet, whereas C_i and m_i are the respective values for ice.

The right-hand-side of Eq. (1) describes the powers involved in the heat exchange processes. The radiation term, P_{rad}, consists of three parts:

$$P_{rad} = (1 - a)S_c R_{sw} + \varepsilon_c S_c R_{lw} - P_c, \quad (2)$$

where R_{sw} and R_{lw} are the solar and thermal components of the incoming radiation from the input reanalysis data (see Table 2), a is the sheet's albedo and ε_c its emissivity (i.e. the absorbed fraction of radiation) in the infra-red band. Note that the effect of cloudiness is indirectly included via the input radiation terms. The outgoing radiative power, P_c, is given by the Stephan–Boltzmann law,

$$P_c = S_c \varepsilon_c \sigma T_c^4, \quad (3)$$

where σ is the Stephan–Boltzmann constant.

Returning to Eq. (1), the convective heat-exchange term, P_{conv}, is given by

$$P_{conv} = S_c h(T_a - T_c), \quad (4)$$

where T_a is the 2 m ambient air temperature and h is the heat transfer coefficient, estimated by

$$h = f\sqrt{u/D}. \quad (5)$$

Here f is an empirical constant, taken to be 4 $W K^{-1} m^{-2} s^{1/2}$ as previously suggested by Pedro and Gillespie (1982), u is the prevailing 2 m horizontal wind speed and $D = \sqrt{S_c}$ is the characteristic length of the sheet (here 1 m).

The final term in Eq. (1), P_{lat}, represents the latent heat released by the condensation/desublimation of water

$$P_{lat} = \begin{cases} L_{vw}\frac{dm_w}{dt} & \text{if } T_c \geq 0\,^\circ C \\ L_{vi}\frac{dm_i}{dt} & \text{if } T_c < 0\,^\circ C, \end{cases} \quad (6)$$

HESSD
11, 9519–9549, 2014

where L_{vw} and L_{vi} are the specific latent heat of vaporisation and desublimation for water, the appropriate one selected based on whether the temperature of the condenser is above or below the freezing point of water. The algorithm imposes a similar condition for dynamically changing the phase of pre-existing water or ice on the condenser sheet: if liquid water exists (i.e. $m_w > 0$) while $T_c < 0$ and the sheet is losing energy (i.e. the right-hand-side of Eq. (1) is negative), instead of solving Eq. (1), the model will keep T_c constant and solve

$$L_{wi}\frac{dm_w}{dt} = P_{rad} + P_{conv} + P_{lat}, \quad (7)$$

where L_{wi} is the latent heat of fusion. The mass of lost (i.e. frozen) water is added to the cumulated mass of ice. A similar equation is solved for m_i in situations when there is ice present on the condenser but the temperature of the condenser is above zero degrees Celsius. Note that Eq. (7) is unrelated to condensation, and only describes the phase transition of already-condensed water or ice.

For the rate of condensation (independent of Eq. 7) we can write a mass balance equation

$$\frac{dm}{dt} = \max(0, S_c k(p_{sat}(T_d) - p_c(T_c))), \quad (8)$$

where m represents either m_i or m_w depending on whether $T_c < 0\,^{\circ}\mathrm{C}$ or not, $p_{sat}(T_d)$ is the saturation pressure at the dew point temperature, $p_c(T_c)$ is the vapour pressure over the condenser sheet and k is a semi-empirical mass transfer coefficient (Pedro and Gillespie, 1982)

$$k = \frac{0.656h}{C_a p}, \quad (9)$$

where p is the atmospheric air pressure and C_a is the specific heat capacity of air. Note that Eq. (8) assumes irreversible condensation, i.e. there is no evaporation or sublimation during daytime even when $T_c > T_a$. This assumption simulates the daily manual

HESSD
11, 9519–9549, 2014

collection of the condensed water around sunrise, soon after which the temperature of the sheet often increases above the dew point temperature. In the model we reset the cumulated values for water and ice at local noon, and take the preceding maximum value of $m_w + m_i$ as the representative daily yield.

In our model we approximate the vapour pressure $p_c(T_c)$ in Eq. (8) by the saturation pressure of water at temperature T_c. In reality, the wettability of the surface affects the vapour pressure p_c directly above it: a wetted surface decreases the vapour pressure, and condensation may take place even if $T_c > T_d$ (Beysens, 1995). Beysens et al. (2005) accounted for this effect by including an additional empirical parameter, T_0, such that $p_c(T_c) = p_{sat}(T_c+T_0)$, and found the optimal value of T_0 to be −0.35 K. However, Beysens et al. (2005) used a collector with a different design to that assumed in this study, a more expensive, 5 mm thick PMMA plate, and we were unable to find a reference value for T_0 valid for LDPE. This simplification causes a small underestimation of the condensation rate calculated by Eq. (8).

The model reads all input data for a given grid point and solves Eqs. (1), (7) and (8) using a 4th order Runge–Kutta algorithm with a 60 s time step. An example case spanning two consecutive days is presented in Fig. 1, which shows the long- and short-wave radiation components, wind speed, air temperature, dewpoint temperature as well as the modelled sheet temperature and cumulated dew. During daytime, the incoming short-wave radiation from the sun as well as the atmospheric long-wave radiation act to increase the temperature of the condenser sheet. In contrast, during dark periods, the outgoing thermal radiation exceeds the atmospheric long-wave radiation, the latter of which is greatly influenced by cloudiness: the thermal emission by clouds, especially low clouds, increases the incoming thermal radiation at the surface. As condensation occurs when the temperature of the condenser sheet is below the dew point temperature (Eq. 8), significant dew cumulation can only occur during night-time. The daily collection of dew occurs at noon, depicted by the dashed vertical lines.

HESSD
11, 9519–9549, 2014

2.2 Meteorological input data

The meteorological input data for the dew formation model is obtained from the European Centre for Medium Range Weather Forecasts (ECMWF) Interim Reanalysis (ERA-Interim, Dee et al., 2011). Reanalysis datasets are produced by combining historical observations from multiple sources with a comprehensive numerical model of the atmosphere using data assimilation systems. As numerical models of the atmosphere are constantly evolving, reanalysis datasets are more appropriate for long term studies than operational analyses as a fixed numerical model is used. Numerous different global reanalysis datasets are available, for example NASA MERRA (Rienecker et al., 2011), JRA-25 (Onogi et al., 2007) and NCEP-CFSR (Saha et al., 2010) and many inter-comparison studies between the different reanalysis datasets have been conducted (e.g. Lorenz and Kunstmann, 2012; Willett et al., 2013; Simmons et al., 2014). ERA-Interim was selected for this study primarily because it is the only available reanalysis which assimilates two-metre temperature and therefore has a lower two-metre temperature bias than any other available re-analysis (Decker et al., 2012).

ERA-Interim is ECMWFs current global reanalysis dataset spanning from 1979–present which has a horizontal resolution of 0.75° (approximately 80 km) and 60 levels in the vertical. We use 34 years (1979–2012) of ERA-Interim data and the variables extracted from ERA-Interim to be applied in the dew formation model are listed in Table 2. The data for wind speed, temperature, and dew point temperature originate from reanalysis fields valid at 00:00, 06:00, 12:00 and 18:00 UTC, while the data valid at 03:00 and 09:00 UTC (15:00 and 21:00 UTC) are forecast fields based on the reanalysis of 00:00 UTC (12:00 UTC). The radiative parameters are purely forecast fields and are cumulative over the forecast period; in this study we derive a simple average from the difference between adjacent cumulative values to obtain instantaneous values.

The dew formation model requires the wind speed at a height of two metres, whereas only the 10 m wind speed is available in the ERA-Interim reanalysis dataset. Therefore, the 2 m wind speed is estimated using the logarithmic wind profile (e.g. Seinfeld and

HESSD
11, 9519–9549, 2014

Pandis, 2006)

$$u = \frac{\log(2/z_0)}{\log(10/z_0)} \sqrt{u_{10,x}^2 + u_{10,y}^2}, \quad (10)$$

where z_0 is the forecast surface roughness taken from the ERA-interim reanalysis data set and $u_{10,x}$ and $u_{10,y}$ are the 10 m horizontal wind speed components.

Even by combining the ERA-Interim forecast fields with the analyses fields, the temporal resolution of the meteorological input data is only three hours. In contrast, the numerical dew formation model requires meteorological input every timestep (60 s). Therefore, the three-hourly ERA-Interim data is linearly interpolated to 60 s time resolution. This is a disadvantage of using reanalysis data compared to using more frequent observations. However, we believe that this disadvantage is considerably outweighed by the advantages of using reanalysis data; the long time series and the uniform global coverage.

3 Results and discussion

Figure 2 illustrates the sensitivity of the modelled dew yield to changes in the emissivity, albedo, and heat capacity of the sheet as well as to the wind speed and the timestep of the model. The dew yield increases almost linearly with the sheet's emissivity, and the emissivity seems to be the most important factor to consider when designing condenser materials (besides economic factors). The albedo of the sheet has a smaller effect as it only affects the sheet's temperature during sunlit hours, when the sheet is anyhow heated convectively by high air temperatures (see Fig. 1). The sheet's heat capacity does not significantly affect the dew yield unless it is either very low or very high (note the logarithmic scale). Interestingly, the issue of heat capacity may have been the key limiting factor in massive ancient dew collection infrastructure (Nikolayev et al., 1996). Note that for the simulated horizontal plane, current technologies already

HESSD
11, 9519–9549, 2014

lie close to optima. The model timestep was chosen to be 60 s as this keeps the model stable even in the very-high-yield scenario of Fig. 2.

Finally, the effect of wind speed is more complex: decreasing the wind speed reduces the mass flow towards the condenser, whereas increasing the wind speed increases convective heating. For this reason, dew collectors should be placed, for example, on elevated structures, so that the average wind speeds during night-time are optimal for dew collection. It should be noted that the model formulation used in this study assumes a constant supply of atmospheric moisture defined by the dew point temperature. In a more realistic scenario, the layer of air directly above the surface of the condenser should eventually dry if both vertical mixing and the horizontal wind speed were small. Although in the model the dew yield does vanish at very small wind speeds, the assumption of a constant moisture supply may become invalid for very large collectors. On the other hand, the potential for dew collection still exists, and when designing large-scale dew collection, passive air-mixers should be introduced to ensure a supply of moist air.

The following results originate from a series of global simulations. The model simulations differ only by the parameters of albedo and emissivity that describe the ability of the condenser's sheet to emit and absorb energy by radiation. Recall that the spatial resolution of the meteorological input data is a relatively coarse, $0.75^{\circ} \times 0.75^{\circ}$ (up to 80 km, depending on latitude), which does limit the model's ability to capture small-scale phenomena such as those caused by local topography. Therefore, this limitation should be considered when interpreting the model results.

Furthermore, Beysens et al. (2005) introduced additional site-specific parameters to the heat and mass transfer coefficients (Eqs. 5, 9) to accommodate for differences in environmental conditions between the condenser surface and the meteorological instruments, as well as a correction in Eq. (8) to account for surface wetting. In our study the difference between the reanalysis data and any real physical location within the area represented by the gridpoint is arguably much greater, but as we see no means to tailor the model separately for each grid point, we use the theoretical formulation as it

HESSD
11, 9519–9549, 2014

is. This assumption will inevitably cause some error in the dew yield estimates, although the large-scale average should be reasonably well predicted.

3.1 Occurrence of dew

First and foremost, it is important to gain insight into how frequently dew forms onto the artificial surface in different areas around the world. Our model results suggest that dew formation is both global and common, with surprisingly little seasonal variation in most areas. Figure 3 presents the mean seasonal fraction of days during which the formation of dew onto the collector occurs (i.e. the yield is positive). Apart from very warm and dry deserts, rainforests, and summer-time polar regions (which experience long days), the meteorological conditions on all continental areas favour the formation of dew onto the collector.

The lack of dew formation is generally caused by inefficient nocturnal cooling of the surface as a result of high incoming long-wave radiation, which occurs due to a high cloud fraction and high humidity in the atmosphere (although high humidity at surface level favours dew formation). This is particularly true for rainforests and the trade wind regions. In forests, the 2 m wind speed may also be close to zero, which prevents dew formation (see Fig. 2). The coastal areas influenced by cold ocean currents seem to be more favorable for dew formation than those influenced by warm ocean currents.

Perhaps somewhat counter-intuitively, in general the artificial surfaces over oceans do not collect dew as regularly as those over land-areas. The relative lack of oceanic dew formation is probably caused by the weaker diurnal cycle in air temperature, denser average cloud-cover (e.g. King et al., 2013) and higher humidity compared to land areas, resulting in amplified long-wave radiation downwards, and therefore weaker cooling.

In most dew events represented by Fig. 3, the cumulated amount of water is insignificant (see Sect. 3.2). Figure 4 shows a similar seasonal occurrence of dew as fraction of days, but only during which more than 0.1 mm d^{-1} (i.e. 0.1 L m^{-2} d^{-1}) can be collected. The contrast between the two figures is notable, as in the latter the seasonal variation

HESSD
11, 9519–9549, 2014

is higher and dew formation occurs regularly in far fewer areas, most of which do not have a water shortage problem. However, in some water-stressed areas, such as the coastal regions of north Africa and the Arabian Peninsula, dew collection may be an alternative source of water worth investigating further.

3.2 Yield of dew

Given the occurrence of dew formation events as presented in Sect. 3.1, we subsequently calculated the mean seasonal values for the actual daily amounts of dew cumulated on the collector sheet. The reported values represent the liquid water-equivalent volumes of the sum of liquid water and ice. For the condenser parameters shown in Table 1, this *dew potential* is presented in Fig. 5. Unsurprisingly, the global distribution of dew potential closely resembles Fig. 4 and indicates that most areas with the potential to harvest non-negligible quantities of dew are also those with sufficient other sources of water. Note the high seasonal variation especially in equatorial Africa, India, the Mediterranean Sea and sourthern Australia.

The standard deviation of the seasonal formation of dew is presented in Fig. 6. The variation is surprisingly zonal compared to Fig. 5. On the other hand, the highest variation is found in regions with the highest dew yields as might be expected. In particular, dew yields in the aforementioned coastal regions of northern Africa and the Arabian Peninsula exhibit high standard deviations, suggesting that if large-scale dew collection in these areas was planned, varying dew yields should be expected.

Figure 7 presents a time series of dew yield in the Negev desert, Israel, where dew collection has been studied by several authors (e.g. Evenari, 1982; Zangvil, 1996; Kidron, 1999; Jacobs et al., 2000). The values from our model are significantly higher than most of the reported values, possibly because the condenser properties assumed in this study are too idealised, although the coarse resolution of our data, as well as the differences in the collection methods, make direct comparison with measurements difficult. Note the decreasing trend in the modelled dew yields in Fig. 7.

HESSD
11, 9519–9549, 2014

3.3 Increase of dew

The data presented in Fig. 4 is for a sheet emissivity of 0.94 and albedo of 0.84, both of which can possibly be improved by means of material science. If both the emissivity and the albedo were hypothetically increased to an extreme value of 0.999, the occurrence of dew would increase as presented in Fig. 8. Although this *ideal collector* scenario is exaggerated, these model results suggest that improvements in the emissivity and albedo could have a significant effect on the sheet's ability to condense water, and thus the cost of a high-performance sheet material may be justified. It should be noted that besides increasing the emissivity and the albedo of the sheet, other means of enhancing the condenser's performance exist as well. For example, Beysens et al. (2013) reported an increase in dew yields of up to 400 % for origami shaped collectors compared to a planar condenser inclined at an angle of 30°.

In general, the ideal condenser scenario suggests that enhancing the properties of the condenser would increase the occurrence of dew most significantly over the oceans, especially in the summer hemisphere. In Antarctica and Greenland, the summer-time dew yields increase significantly over the subjective 0.1 mm d^{-1} limit in the ideal condenser scenario, which results in these regions being highlighted in Fig. 8.

The absolute increase in the mean seasonal formation of dew is presented in Fig. 9, suggesting that the dew yield can be up to doubled in some areas in this extreme scenario. In general, however, the increase in the absolute dew yield is relatively small even in areas where enhancing the condenser's properties significantly increases dew occurrence. This implies that the relative importance of different factors affecting dew formation varies globally, and that radiative cooling is the main limiting factor, for example, in the Mediterranean Sea.

3.4 Trend of dew

With the projected changes in climate and potentially increasing occurrences of drought (Stocker, 2013), we investigated the existence of temporal trends in the

HESSD
11, 9519–9549, 2014

modelled dew yields. Trends were calculated by applying the Mann–Kendall (i.e. Kendall Tau-b) trend test (e.g. Agresti, 2010) on seasonal means of yearly data. Unsurprisingly, the statistical significance of the trends vary non-uniformly across the globe. Nevertheless, in some regions a statistically significant trend ($p < 0.05$) is found.

Figure 10 presents the overall change in the mean seasonal formation of dew. Only statistical significant ($p < 0.05$) changes are shown, with the trend being equal to the Theil–Sen estimator (Theil, 1950; Sen, 1968). Interestingly, the general trend appears to indicate a decrease in dew potential in most water-stressed areas. The changes appear in large and roughly uniform areas, suggesting that the phenomenon cannot be entirely attributed to noise. A significant decreasing trend is also visible in the case study presented in Fig. 7. In addition, a decreasing trend is also visible in the coastal regions of northern Africa and the Arabian Peninsula, which we identified as regions of high dew collection potential (see previous sections).

4 Conclusions

The global potential for collecting dew on artificial surfaces was investigated by implementing a dew formation model based on solving the heat and mass balance equations. As meteorological input, 34 years of global reanalysis data from ECMWF's ERA-Interim archive was used.

Dew formation was found to be common and frequent, though mostly over land-areas where other sources of water exist. Nevertheless, some water-stressed areas, especially the coastal regions of northern Africa and the Arabian Peninsula might be suitable for economically viable large-scale dew collection, as the yearly yield of dew can exceed 100 L m^{-2} for a commonly used LDPE foil. For these locations, more accurate regional modelling and field experiments should be conducted.

The long time series provides some statistical confidence in conducting a trend analysis, and it suggests significant changes in dew yields in some areas in the range of ±15 % over the investigated time period.

HESSD
11, 9519–9549, 2014

It should be noted that the real-life usefulness of the results presented in this paper depends on several factors not accounted for in this study, such as other sources of water (precipitation, lakes, rivers, desalination of sea-water), pipelines, and road-access to the location for transportation of water by trucks, as well as financial and technological considerations.

Acknowledgements. Funding from the Academy of Finland is gratefully acknowledged (Development of cost-effective fog and dew collectors for water management in semiarid and arid regions of developing countries (DF-TRAP), project No. 257382, as well as Centre of Excellence, project No. 272041). We acknowledge CSC – IT Center for Science Ltd. for the allocation of computational resources. Technical support and performance tips with large NetCDF files from Russell Rew at Unidata is acknowledged.

References

Agresti, A.: Analysis of Ordinal Categorical Data, Vol. 656, John Wiley & Sons, New York, 2010. 9533

Beysens, D.: The formation of dew, Atmos. Res., 39, 215–237, 1995. 9526

Beysens, D., Muselli, M., Nikolayev, V., Narhe, R., and Milimouk, I.: Measurement and modelling of dew in island, coastal and alpine areas, Atmos. Res., 73, 1–22, 2005. 9522, 9523, 9526, 9529

Beysens, D., Brogginib, F., Milimouk-Melnytchoukc, I., Ouazzanid, J., and Tixiere, N.: New architectural forms to enhance dew collection, Chem. Eng., 34, 79–84, 2013. 9532

Clus, O.: Condenseurs radiatifs de la vapeur d'eau atmosphérique (rosée) comme source alternative d'eau douce, Ph. D. thesis, Université Pascal Paoli, 2007. 9538

Decker, M., Brunke, M. A., Wang, Z., Sakaguchi, K., Zeng, X., and Bosilovich, M. G.: Evaluation of the reanalysis products from GSFC, NCEP, and ECMWF using flux tower observations, J. Climate, 25, 1916–1944, 2012. 9527

Dee, D. P., Uppala, S. M., Simmons, A. J., Berrisford, P., Poli, P., Kobayashi, S., Andrae, U., Balmaseda, M. A., Balsamo, G., Bauer, P., Bechtold, P., Beljaars, A. C. M., van de Berg, L., Bidlot, J., Bormann, N., Delsol, C., Dragani, R., Fuentes, M., Geer, A. J., Haimberger, L., Healy, S. B., Hersbach, H., Hólm, E. V., Isaksen, L., Kållberg, P., Köhler, M., Matricardi, M.,

McNally, A. P., Monge-Sanz, B. M., Morcrette, J.-J., Park, B.-K., Peubey, C., de Rosnay, P., Tavolato, C., Thépaut, J.-N., and Vitart, F.: The ERA-Interim reanalysis: configuration and performance of the data assimilation system, Q. J. Roy. Meteor. Soc., 137, 553–597, 2011. 9527

Evenari, M.: The Negev: The Challenge of a Desert, Harvard University Press, 1982. 9531

Fessehaye, M., Abdul-Wahab, S. A., Savage, M. J., Kohler, T., Gherezghiher, T., and Hurni, H.: Fog-water collection for community use, Renew. Sust. Energ. Rev., 29, 52–62, 2014. 9521

Jacobs, A. F., Heusinkveld, B. G., and Berkowicz, S. M.: Dew measurements along a longitudinal sand dune transect, Negev Desert, Israel, Int. J. Biometeorol., 43, 184–190, 2000. 9531

Kidron, G. J.: Altitude dependent dew and fog in the Negev Desert, Israel, Agr. Forest Meteorol., 96, 1–8, 1999. 9531

King, M. D., Platnick, S., Menzel, W. P., Ackerman, S. A., and Hubanks, P. A.: Spatial and temporal distribution of clouds observed by MODIS onboard the Terra and Aqua satellites, IEEE T. Geosci. Remote, 51, 3826–3852, 2013. 9530

Klemm, O., Schemenauer, R. S., Lummerich, A., Cereceda, P., Marzol, V., Corell, D., van Heerden, J., Reinhard, D., Gherezghiher, T., Olivier, J., Osses, P., Sarsour, J., Frost, E., Estrela, M. J., Valiente, J. A., and Fessehaye, G. M.: Fog as a fresh-water resource: overview and perspectives, Ambio, 41, 221–234, 2012. 9521

Lorenz, C. and Kunstmann, H.: The hydrological cycle in three state-of-the-art reanalyses: intercomparison and performance analysis, J. Hydrometeorol., 13, 1397–1420, 2012. 9527

Nikolayev, V., Beysens, D., Gioda, A., Milimouk, I., Katiushin, E., and Morel, J.: Water recovery from dew, J. Hydrol., 182, 19–35, 1996. 9523, 9528

Nilsson, T., Vargas, W., Niklasson, G., and Granqvist, C.: Condensation of water by radiative cooling, Renew. Energ., 5, 310–317, 1994. 9523, 9538

Onogi, K., Tsutsui, J., Koide, H., Sakamoto, M., Kobayashi, S., Hatsushika, H., Matsumoto, T., Yamazaki, N., Kamahori, H., Takahashi, K., Kadokura, S., Wada, K., Kato, K., Oyama, R., Ose, T., Mannoji, N., and Taira, R.: The JRA-25 reanalysis, J. Meteorol. Soc. Jpn., 85, 369–432, 2007. 9527

Pedro, M. J. and Gillespie, T. J.: Estimating dew duration. 1. Utilizing micrometeorological data, Agr. Meteorol., 25, 283–296, 1982. 9523, 9524, 9525

Rienecker, M. M., Suarez, M. J., Gelaro, R., Todling, R., Bacmeister, J., Liu, E., Bosilovich, M. G., Schubert, S. D., Takacs, L., Kim, G.-K., Bloom, S., Chen, J., Collins, D.,

HESSD
11, 9519–9549, 2014

Conaty, A., da Silva, A., Gu, W., Joiner, J., Koster, R. D., Lucchesi, R., Molod, A., Owens, T., Pawson, S., Pegion, P., Redder, C. R., Reichle, R., Robertson, F. R., Ruddick, A. G., Sienkiewicz, M., and Woollen, J.: MERRA: NASA's modern-era retrospective analysis for research and applications, J. Climate, 24, 3624–3648, 2011. 9527

Saha, S., Moorthi, S., Pan, H.-L., Wu, X., Wang, J., Nadiga, S., Tripp, P., Kistler, R., Woollen, J., Behringer, D., Liu, H., Stokes, D., Grumbine, R., Gayno, G., Wang, J., Hou, Y.-T., Chuang, H.-Y., Juang, H.-M. H., Sela, J., Iredell, M., Treadon, R., Kleist, D., Van Delst, P., Keyser, D., Derber, J., Ek, M., Meng, J., Wei, H., Yang, R., Lord, S., Van Den Dool, H., Kumar, A., Wang, W., Long, C., Chelliah, M., Xue, Y., Huang, B., Schemm, J.-K., Ebisuzaki, W., Lin, R., Xie, P., Chen, M., Zhou, S., Higgins, W., Zou, C.-Z., Liu, Q., Chen, Y., Han, Y., Cucurull, L., Reynolds, R. W., Rutledge, G., and Goldberg, M.: The NCEP climate forecast system reanalysis., B. Am. Meteorol. Soc., 91, 1015–1057, 2010. 9527

Schemenauer, R. S. and Cereceda, P.: Fog-Water collection in arid coastal locations, Ambio, 20, 303–308, 1991. 9521

Seinfeld, J. H. and Pandis, S. N.: Atmospheric Chemistry and Physics, John Wiley & Sons, New York, 2006. 9527

Sen, P. K.: Estimates of the regression coefficient based on Kendall's tau, J. Am. Stat. Assoc., 63, 1379–1389, 1968. 9533

Simmons, A. J., Poli, P., Dee, D. P., Berrisford, P., Hersbach, H., Kobayashi, S., and Peubey, C.: Estimating low-frequency variability and trends in atmospheric temperature using ERA-Interim, Q. J. Roy. Meteor. Soc., 140, 329–353, 2014. 9527

Stocker, T. F., Qin, D., Plattner, G.-K., Tignor, M., Allen, S. K., Boschung, J., Nauels, A., Xia, Y., Bex, V., and Midgley, P. M.: Climate change 2013: The physical science basis, Intergovernmental Panel on Climate Change, Working Group I Contribution to the IPCC Fifth Assessment Report (AR5)(Cambridge Univ Press, New York), 2013. 9532

Theil, H.: A rank-invariant method of linear and polynomial regression analysis, Part 3, Proceedings of Koninalijke Nederlandse Akademie van Weinenschatpen A, 53, 1397–1412, 1950. 9533

United Nations Development Programme: Human Development Report 2006, Beyond Scarcity: Power, Poverty and the Global Water Crisis, Palgrave Macmillan, New York, 2006. 9520

Vogt, M., Vuollekoski, H., Petäjä, T., Ahokas, J., Korpela, A., Vähä-Nissi, M., Sipilä, M., Lappalainen, H., and Kulmala, M.: Dew harvesting by radiative cooling: A review of promising water resource for florae and society, in review, 2014. 9521

HESSD
11, 9519–9549, 2014

Willett, K. M., Dolman, A. J., Hall, B. D., and Thorne, P. W. (Eds.): Global climate, in: State of the Climate in 2012, Vol. 94, B. Am. Meteorol. Soc., S7–S46, 2013. 9527
Zangvil, A.: Six years of dew observations in the Negev Desert, Israel, J. Arid Environ., 32, 361–371, 1996. 9531

HESSD
11, 9519–9549, 2014

Table 1. Some parameters used in the model, unless specified otherwise. The properties of the foil are for common low-density polyethylene with composition according to Nilsson et al. (1994) and radiative properties as found by Clus (2007).

Parameter	Value
Sheet density ρ_c	$920\,\mathrm{kg\,m^{-3}}$
Sheet thickness δ_c	0.39 mm
Sheet specific heat capacity C_c	$2300\,\mathrm{J\,kg^{-1}\,K^{-1}}$
Sheet IR emissivity e	0.94
Sheet short-wave albedo a	0.84
Timestep	60 s

HESSD
11, 9519–9549, 2014

Table 2. The data acquired from the ECMWF's ERA-Interim database.

Original parameter	Derived model input
10 m U wind component	Wind speed
10 m V wind component	
Forecast surface roughness	
2 m temperature	Air temperature
2 m dew point temperature	Dew point
Surface solar radiation downwards	Short-wave radiation in
Surface thermal radiation downwards	Long-wave radiation in

HESSD
11, 9519–9549, 2014

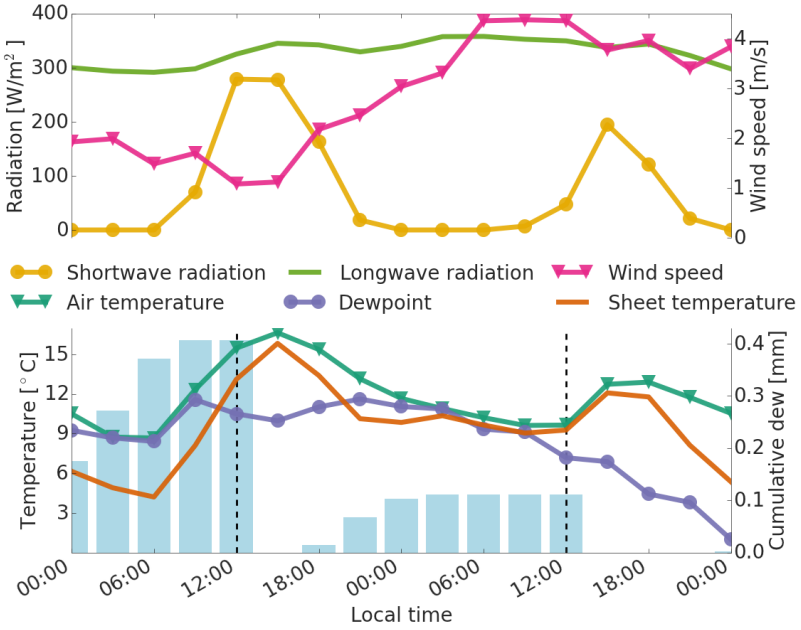

Figure 1. An example of modelled dew formation events on two consecutive days in September 2000 in Helsinki, Finland. The short-wave and long-wave radiation, wind speed, air temperature and dew point are input from the ERA-Interim dataset. Note that the amount of dew is reset daily at local noon (dashed vertical lines). All data is in 3 h resolution.

HESSD
11, 9519–9549, 2014

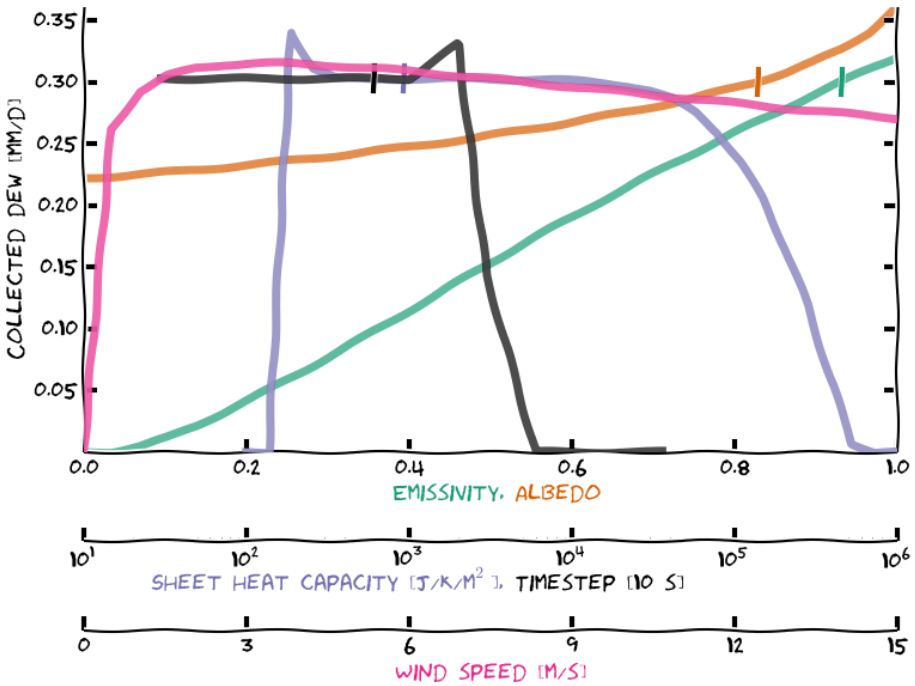

Figure 2. Sensitivity of the model to the emissivity, albedo and heat capacity of the condenser sheet as well as to the wind speed and timestep of the model (×10 in figure). The heat capacity is defined here as $C_c\rho_c S_c\delta_c$ i.e. its variation corresponds to varying any of these factors. The input data corresponds to Table 1 and the first day of Fig. 1, where applicable. The vertical bars represent these *default* values.

HESSD
11, 9519–9549, 2014

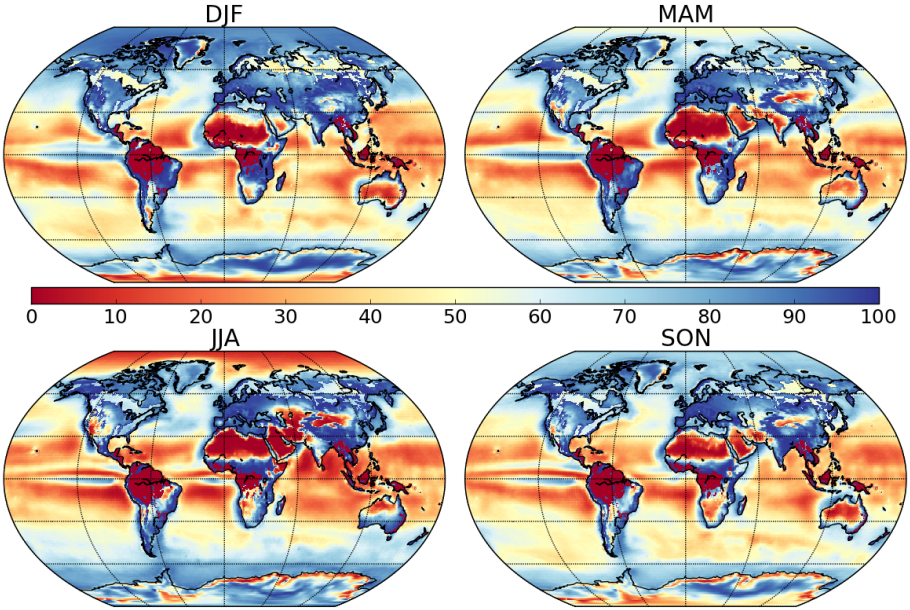

Figure 3. Seasonal occurrence of dew as a fraction of days (%).

HESSD
11, 9519–9549, 2014

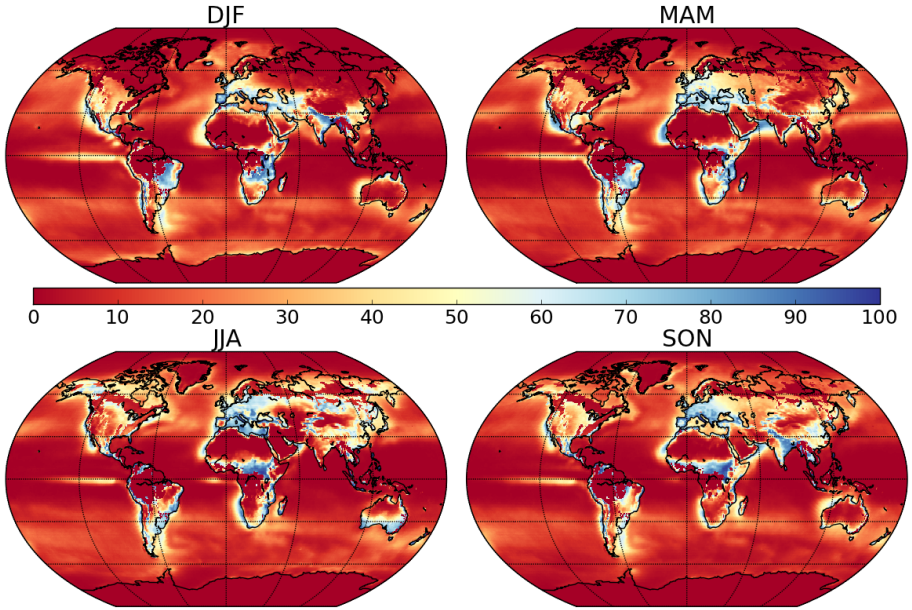

Figure 4. Seasonal occurrence of dew as a fraction of days (%) with a threshold of 0.1 mm d^{-1}.

HESSD
11, 9519–9549, 2014

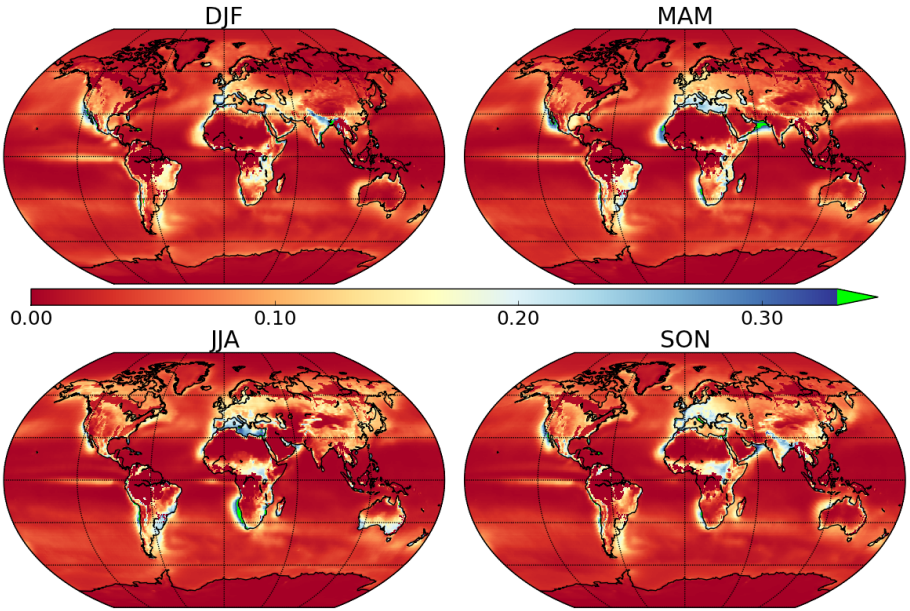

Figure 5. Mean seasonal formation of dew (mm d^{-1}).

HESSD
11, 9519–9549, 2014

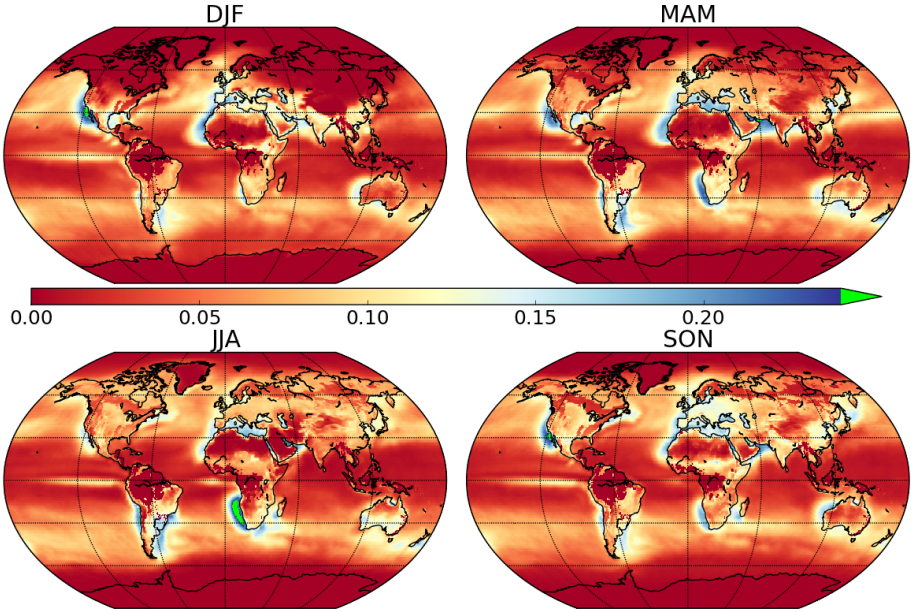

Figure 6. Standard deviation of the seasonal formation of dew (mm d^{-1}).

HESSD
11, 9519–9549, 2014

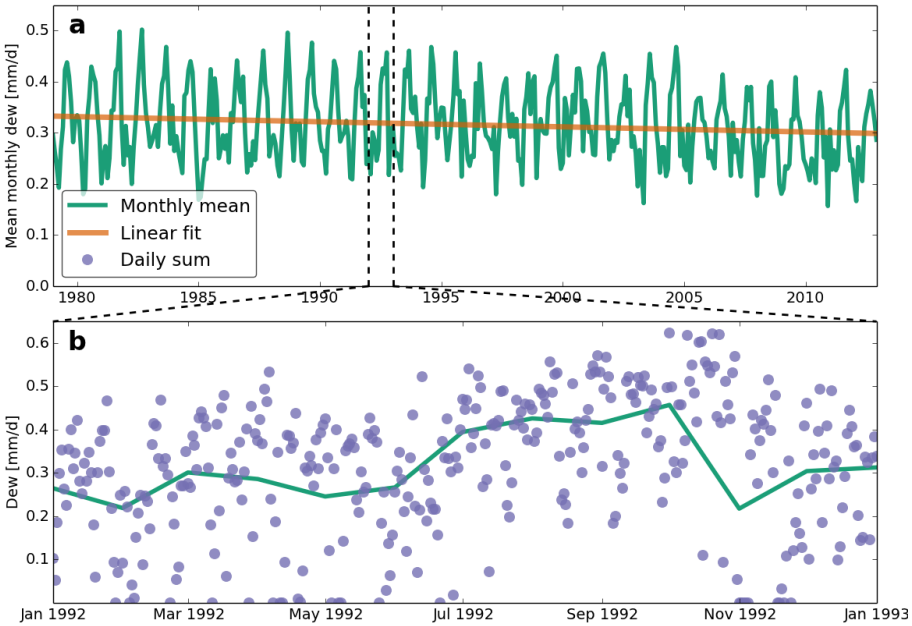

Figure 7. Time series of the modelled dew yield from one grid point, 30.75° N, 34.5° E, located in the Negev desert, Israel: **(a)** the monthly means over the whole dataset, as well as a linear fit to the data; **(b)** the monthly means as well as daily values for the year 1992.

HESSD
11, 9519–9549, 2014

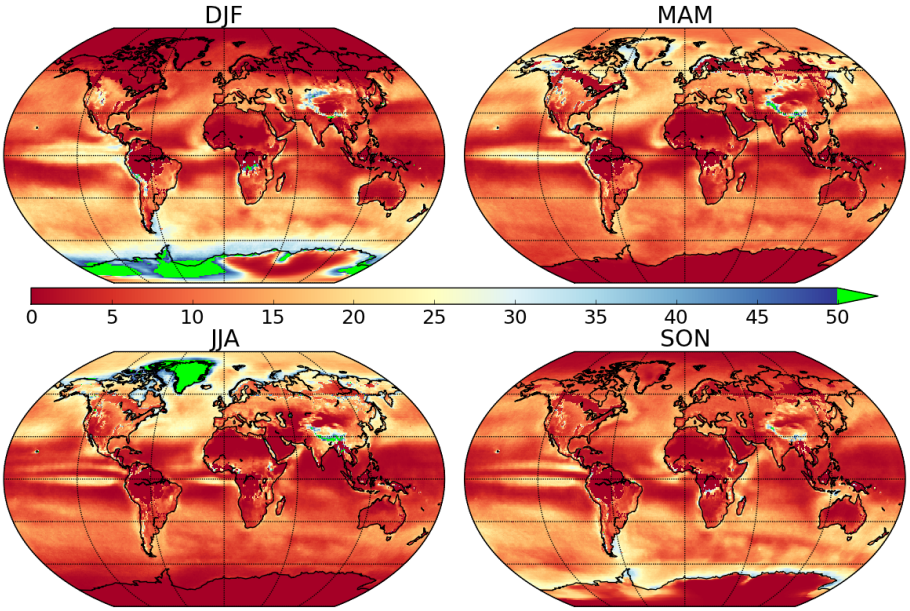

Figure 8. The fractional increase in the seasonal occurrence of dew (%) with a threshold of 0.1 mm d^{-1}, when the emissivity of the condenser is increased from 0.94 to 0.999, and the albedo from 0.84 to 0.999.

HESSD
11, 9519–9549, 2014

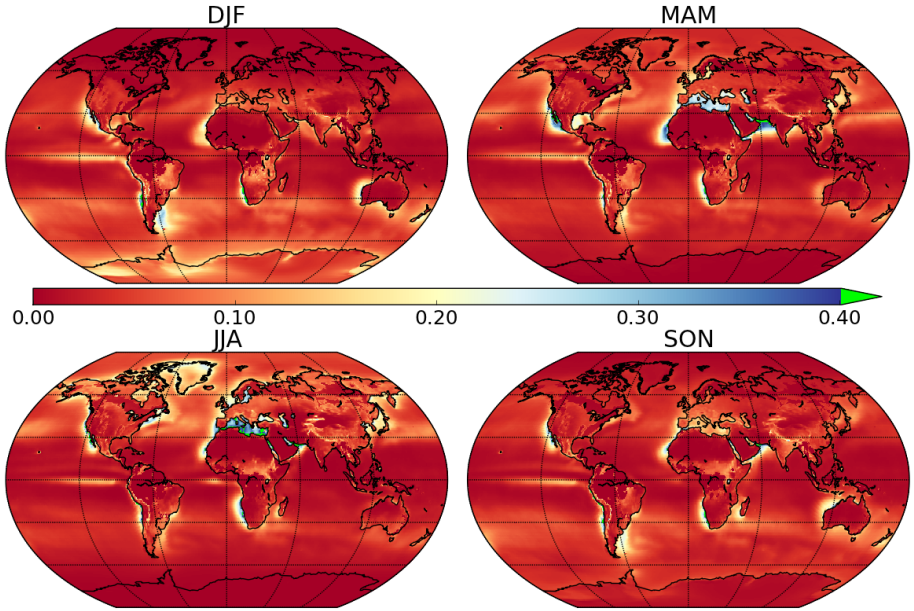

Figure 9. The absolute increase in the mean seasonal formation of dew (mm d^{-1}), when the emissivity of the condenser is increased from 0.94 to 0.999, and the albedo from 0.84 to 0.999.

HESSD
11, 9519–9549, 2014

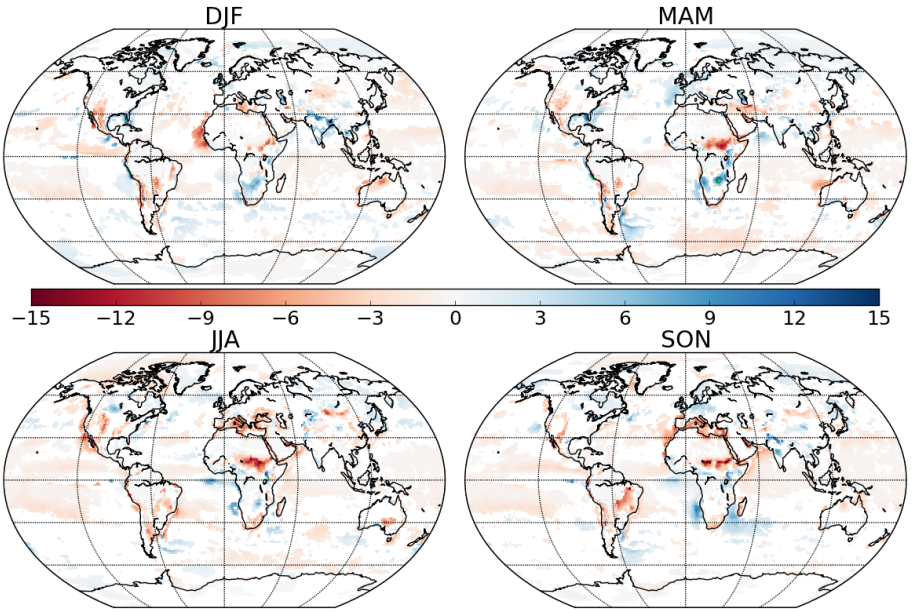

Figure 10. The total change (%) in the mean seasonal formation of dew (mm d^{-1}) over the years 1979–2012 as predicted by the Theil–Sen estimator. Only locations with a statistically significant trend ($p < 0.05$) are shown.

HESSD
11, 9519–9549, 2014